Journal Pre-proofs

Boosting Transdermal delivery of Atorvastatin Calcium *via* o/w Nanoemulsifying System: Two-step optimization, *ex vivo* and *in vivo* evaluation

Dalia S. Shaker, Rania A.H. Ishak, Muaeid A. Elhuoni, Amira M. Ghoneim

PII: S0378-5173(20)30057-0
DOI: https://doi.org/10.1016/j.ijpharm.2020.119073
Reference: IJP 119073

To appear in: *International Journal of Pharmaceutics*

Received Date: 9 December 2019
Revised Date: 19 January 2020
Accepted Date: 20 January 2020

Please cite this article as: D.S. Shaker, R.A.H. Ishak, M.A. Elhuoni, A.M. Ghoneim, Boosting Transdermal delivery of Atorvastatin Calcium *via* o/w Nanoemulsifying System: Two-step optimization, *ex vivo* and *in vivo* evaluation, *International Journal of Pharmaceutics* (2020), doi: https://doi.org/10.1016/j.ijpharm.2020.119073

Boosting Transdermal delivery of Atorvastatin Calcium *via* o/w Nanoemulsifying System: Two-step optimization, *ex vivo* and *in vivo* evaluation

Dalia S. Shaker[a], Rania A. H. Ishak[b], Muaeid A Elhuoni[c], Amira M. Ghoneim[a] *

[a] *Department of Pharmaceutics &Pharmaceutical Technology, Faculty of Pharmaceutical Sciences and Pharmaceutical industries, Future University in Egypt (FUE), Cairo, Egypt.*

[b] *Department of Pharmaceutics & Industrial Pharmacy, Faculty of Pharmacy, Ain Shams University, Cairo, Egypt.*

[c] *Quality Control Department, Elnajah Medical Services, Benghazi, Libya.*

* Corresponding to:

Amira M. Ghoneim, PhD.
Department of Pharmaceutics &Pharmaceutical Technology, Faculty of Pharmaceutical Sciences and Pharmaceutical industries, Future University in Egypt (FUE), Cairo, Egypt Tel: (202) - 241-42927
Fax: (202) -2618-6111
P.O. Box: 11477

Email: amiraghoneim@gmail.com

Emails of Co-authors

- Dalia S. Shaker: dalia.samuel@fue.edu.eg

- Rania A.H. Ishak: raniaaziz@pharma.asu.edu.eg

- Muaeid A. Elhuoni: Moaid.pharm@gmail.com

Abstract

A nanoemulsion system was designed for Atorvastatin calcium (ATOR) transdermal delivery to overcome its poor bioavailability of (30%) resulting from the extensive first-pass effect and dissolution rate-limited *in vivo* absorption. Pseudo ternary phase diagrams were developed, and various NE formulae were prepared using oleic acid (OA), Tween 80 as surfactant and PEG 400 as cosurfactant, ethanol and limonene as permeation enhancers (PEs). NEs were characterized for morphology, droplet size, zeta potential and *in vitro* release. The optimized formulae were assessed for *ex vivo* transdermal permeation and *in vivo* pharmacodynamic/ pharmacokinetic studies. Hypocholesterolemic effect after 7 days skin treatment was detected and compared to oral ATOR dispersion. Finally, blood plasma levels were measured for 24 hr for rats received the selected transdermal NE and transdermal drug in OA. The obtained results suggested the low potentiality of NE systems in transdermal delivery of lipophilic drugs, only the addition of PEs is driving factor for increasing drug flux through full thickness rat skin. In the optimized formula, the presence of ethanol and PEG 400 disrupts SC lipids exhibiting rapid *ex vivo* release profile compared to other NEs and to ATOR in OA. In contrast, the optimized NE achieved a prolonged plasma profile. Transdermal NE was significantly more efficient than oral administration in lowering cholesterol plasma level and in increasing ATOR bioavailability. In conclusion, data revealed no correlation between *ex vivo* and *in vivo* studies explained by the collapse of the follicles in *ex vivo* skin permeation study, leaving only the lipoidal pathway for NE to pass through, thus only NE components, neither nanosizing nor other reported mechanisms, are the main influencing factors. *In vivo* experiments suggested that o/w NE changed ATOR pathway to follicular delivery leading to accumulation of NE in follicles and consequently a prolonged plasma profile.

Keywords

Atorvastatin calcium; Transdermal nanoemulsion; Hypocholesterolemic effect; Permeation enhancers; *ex vivo* and *in vivo* correlation

Chemical compounds stated in this article

Atorvastatin Calcium (PubChem CID: 60822); Tween 20 (PubChem CID: 443314); Tween 80 (PubChem CID: 5284448); d- Limonene (PubChem CID: 440917). Oleic acid (PubChem CID: 445639); Polyethylene Glycol (PubChem CID: 174).

1. Introduction

Atorvastatin calcium (ATOR), a 3-hydroxy-3-methylglutaryl-coenzyme A (HMG-CoA) reductase inhibitor, efficiently acts by competitively inhibiting the reductase enzyme which

converts HMG-CoA to mevalonate, thus interfering with cholesterogenesis in the liver. It also decreases the level of low density lipoproteins (LDL) by increasing its reuptake and degradation **(Schachter, 2005)**. Therefore, it has been shown to decrease the progression of coronary atherosclerosis, by shrinking the lipid core of the plaque. In addition to its hypocholesteremic activity, it is used in the mediation of osteoporosis, benign prostatic hyperplasia, and Alzheimer's disease **(Davies et al., 2016)**.

ATOR is a BCS class II compound of low water solubility (log P = 5.39) and high permeability. It has a poor oral bioavailability of only 12-14%, this is mainly attributed to high pre-systemic gastrointestinal clearance, incomplete intestinal absorption and first-pass metabolism **(Adams et al., 2015)**. The oral administration of ATOR also suffers from gastrointestinal disturbances as diarrhea, constipation and decreased appetite **(Ramadan et al., 2015)**. The concomitant intake of food produces a 25 and 9% reduction in maximum drug concentration (C_{max}) and systemic availability, respectively. Due to its extensive hepatic metabolism after oral administration, more oxidative stress is exerted on the liver, this puts patients with liver diseases at risk, taking into consideration the chronic nature of the disease, therefore an alternative route of administration than the oral one could greatly reduce the amount of such metabolic stress on the liver **(Chojnacki et al., 2017).**

The transdermal route would be considered advantageous to improve ATOR bioavailability by avoiding pre-mature drug metabolism in intestine and liver **(Doherty and Pang, 1997)**. In addition, the convenience and ease of application could add to the benefit of this delivery way, which results in better patience compliance. However, the major limiting factor of drug delivery through the skin is to enable the permeation through the stratum corneum (SC), which acts as a natural protective barrier against environmental elements and foreign chemicals. Effectual alteration of such barrier in a reversible manner could resolve this limitation taking into account the hydrophobic compact nature of SC, this could be accomplished *via* well-designed drug delivery platforms.

Nanoemulsion (NE) is a kinetically stable system that consists of two immiscible liquids (oil and water) stabilized by a blend of surfactant and co-surfactant. Nanoemulsions (NEs) are translucent in appearance with droplet size ranged from 20 to 200 nm **(Thakur et al., 2012)**. NEs provide many benefits over other nanocarriers, including simplicity of formulation without the need of high energy or sophisticated procedures, cost-effective, good storage stability, and high drug loading capacity; all of these benefits support scaling up and economic mass production **(Çinar, 2017)**.

To our best knowledge, transdermal delivery of ATOR from NE has not been investigated and only few reports investigated the transdermal delivery of ATOR from transfersomes **(Mahmoud, et al., 2017)**, nanosuspension (**Subramanian, et al., 2016)**, ethosomes (**Bhagya, 2018)** and proniosomes (**Soujanya et al., 2019).**

Herein, different ATOR-loaded o/w NEs were developed, optimized in two steps, and fully characterized. The *ex-vivo* drug permeation across rat skin was studied for the optimized formulations. The selected ATOR-loaded NEs were evaluated *in vivo* compared to oral ATOR. The hypocholesteremic effect of ATOR and its bioavailability from different preparations were assessed *via* PD and PK studies, respectively, allowing to answer the question; by which mechanism does an o/w NE enhance the transdermal permeation of a lipophilic drug?

2. Materials and methods

2.1. Materials

Atorvastatin calcium (purity 98.9%) was kindly gifted by Egyptian International Pharmaceuticals Industries Co. (E.I.P.I.Co, Cairo, Egypt). Tween 80 (polyoxyethylene sorbitan mono oleate), Tween 20 (Polyethylene glycol sorbitan monolaurate), PEG 400 (polyethylene glycol 400), oleic acid, diethyl ether, dichloromethane and ammonium formate were purchased from Oxford Chemicals (Mumbai, India). Captex® 355 EP/NF (triglycerides of caprylic/capric acid) was received as a gift sample from ABITEC Corporation (Ohio, USA). Ethanol (HPLC

grade), Methanol (HPLC grade), acetonitrile (HPLC grade), sunflower oil and cotton seed oil were purchased from Sigma Aldrich (St. Louis, Missouri, USA). D-Limonene was bought from Thermo Fisher (Kandel) GmbH (Karlsruhe, Germany). Disodium hydrogen phosphate, potassium dihydrogen phosphate and sodium chloride were supplied from El-Nasr Pharmaceutical chemicals (Cairo, Egypt). Simvastatin as internal standard was supplied by Ranbaxy (Sungai Petani, Malaysia). Xyla-ject (Xylazine Hydrochloride 23.3 mg/ml) was purchased from Adwia Pharmaceuticals (Cairo, Egypt). Cholesterol measuring kit, Liquizyme single reagent was purchased from Spectrum Diagnostics (Cairo, Egypt). ARcare® 8311, a skin-friendly pressure-sensitive adhesive was purchased from Adhesives Research Ltd. (Essex, UK). Other chemicals and solvents were of analytical grade.

2.2. Methods

2.2.1. Solubility study of ATOR in different oils

In order to select the best oil for NE preparation, the saturated solubility of ATOR was determined according to the method reported by **(Rodde *et al*., 2014)**. Excess amount of the drug was dissolved in 2 ml of various oils, namely; oleic acid, Captex®, cotton seed oil and sunflower oil, in a 5 ml capacity stopper vials. The vials were firmly closed and were mixed continuously for 48 h in mechanical shaker (KS 4000 from IKA, Beijing, China) at 25˚C. Samples were taken from each vial and then subjected to centrifugation at 5000 rpm for 15 min using a cooling centrifuge (Sigma Laborzentrifugen GmbH, Osterode, Germany). The supernatant was collected and filtered with 0.45 µm membrane filter (Thomas Scientific Philadelphia, USA.) then dissolved in methanol and solubility was measured by UV-Vis spectroscopy (Shimadzu UV-Vis spectrophotometer 240j/PC, Tokyo, Japan) at λ_{max} 247 nm after adequate dilution with methanol to determine the maximum ATOR amount solubilized in each component.

The molar extinction coefficient (ε) of ATOR was determined at its λ_{max} in different media used; 100% methanol (for solubility studies) and phosphate buffer saline (PBS) (for *in vitro*

release studies) from Beer's Lambert law and found to be 21564 and 20726 L. mol $^{-1}$.cm^{-1}, respectively.

2.2.2. Construction of pseudo-ternary phase diagrams

The pseudo-ternary phase diagrams were created using water titration method at room temperature, to study the behavior of systems consisting of oil, surfactant/co-surfactant mixture (Smix) and water. Each triangle vertex in the phase diagram represents 100% of each component. Surfactants and co-surfactant (Smix), composed of either Tween 80 or Tween 20 as surfactants and PEG 400 as a co-surfactant, were mixed at different ratios (1:1, 2:1 and 3:1). Mixture of the oil and Smix was prepared at ratios (w/w) of 10:0, 9:1, 8:2, 7:3, 6:4, 5:5, 4:6, 3:7, 2:8, 1:9, 0:10. Double distilled water was added dropwise followed by mixing until the system produced a sudden turbidity followed by transparent appearance indicating the successful formation of NE as described by **(Chavhan *et al.*, 2013)**. The phase diagrams were plotted using Triplot 4.1.2 software (Todd A. Thompson USA), all the studies were repeated in triplicate.

2.2.3. Preparation of ATOR-loaded NEs

Following the identification of the NE regions through the phase diagrams, a series of NE formulae were developed by water titration method using double distilled water as described before, then 20 mg of ATOR was incorporated in the prepared NE and the formula was mixed using a vortex mixer (Heidolph, Germany) NEs were then stored at room temperature until used.

2.2.4. Characterization of ATOR-loaded NEs

2.2.4.1. Measurement of Droplet size, polydispersity index (PDI) and zeta potential (ZP)

One gram of NE formula containing 20 mg of ATOR was diluted to 10 mL with distilled water in a vial and mixed gently. The droplet size and PDI of the NE formulae were determined using dynamic light scattering (DLS), while the ZP of all prepared formulae were measured using laser Doppler anemometry (LDA) technique, both parameters were measured using a Malvern Zetasizer

Nano-ZS instrument (Malvern instruments Ltd. Worcestershire, UK). Light scattering was maintained at 25 ˚C at a 90˚ angle **(Suyal and Ganesh, 2017, Chavhan *et al.*, 2013).**

2.2.4.2. *In vitro* ATOR release study

In vitro release of ATOR was carried out for the selected NE formulae based on the constructed phase diagrams. The study was performed in Franz diffusion cells, using cellulose dialysis membrane with a molecular weight cutoff of 12,000–14,000 Da (Thomas Scientific, Philadelphia, USA). Each cell contains an effective permeation area of 2.27 cm^2 with a receptor chamber volume of 7 mL, equipped with a magnetic stirrer rotating at 600 rpm. The temperature was maintained at 37 ± 0.5 °C. Freshly PBS (500 mL, pH 7.4) was added to the system tank, which is equipped with an automatic sampler and receptor chamber volume replenishing mechanism. The automatic sampler was set to sample and replace receptor volume at intervals of 1, 2, 3, 4, 5, 6, 7 and 8 h, automatically placing the withdrawn sample in a number coded rack for each cell. Analysis of drug concentration was performed using a UV-Vis Spectrophotometer at λ_{max} 247 nm. *In vitro* drug release profiles were plotted as the cumulative percent of drug released against time for all the investigated formulae and the release efficiency (RE_{8h}) was calculated to compare the release profile of all formulae by the following equation:

$$RE = \frac{\int_0^t y.dt}{y_{100}.T} x100 \qquad \text{Eq. (1)}$$

Where ($\int_0^t$y.dt x 100) is the area under curve in an interval of time t, expressed in percentage value and (Y_{100}.T) is the rectangle area considering 100% release in the same time t.

2.2.4.3. Transmission electron microscopy (TEM)

Morphology of the optimized NE formulae was visualized using TEM (JEM-2100, Jeol, Tokyo, Japan). A combination of bright field imaging with escalating magnification and of diffraction modes was utilized to show the shape and size of the NE. A droplet of each selected NE

formula was applied on a copper grid. After formation of a thin film layer, the grid is rinsed to remove non-adherent particles, negatively stained with 1% of phosphotungstic acid, rinsed a second time, and then allowed to dehydrate for 10 min. Once the copper grid was inserted into the TEM electron chamber, an image was formed from the interaction of the electrons transmitted through the NE sample. The image was magnified and focused onto an imaging device, where it was viewed on a computer monitor.

2.2.4.4. Viscosity determination

The viscosity of optimized NE was investigated using Brookfield cone and plate rheometer (Brookfield cone and plate rheometer, Massachusetts, USA) at 25 ± 0.5°C. The sample size/wt was 0.5 g at speed of 30 rpm. Data interval and the loop start were 1, while the wait time was 30 min **(Bhatt and Madhav, 2011).**

2.2.5. *Ex vivo* ATOR skin permeation study

Skin ATOR permeation study was carried out for the optimized NE formulations according to guidelines of Research Ethics Committee of Faculty of Pharmaceutical Sciences & Pharmaceutical Industries, Future University in Egypt (FUE) No (REC-FPSPI-7/46). The rats were first euthanized by use of overdose of sodium thiopental followed by removing the abdominal hair by shaving with electric shaver. Once all the hair was removed, the full-thickness skin was extracted and inspected for scratches, bites or any abnormalities before proceeding to remove the subcutaneous fat carefully without damaging the epidermis, the skin was then placed in PBS solution for 10 min before conducting the experiment. When the skin was not used, it was stored at −20°C and utilized in a period of 1 week of skin harvest. Preceding to testing, the skin was left to thaw in room temperature then equilibrated in PBS (pH 7.4) for 1 h prior to the experiment.

The full thickness skin was positioned onto a receptor compartment with the SC facing the donor chamber, the formulae were then added into each Franz cell (Hanson research, Vision

Microelle autosampler, 6-Cell drive system, autofill collector system, California, USA). The device was set to the desired sampling hours; 2, 4, 8, 12, and 24 h. Samples were then collected and measured *via* HPLC for drug concentration. The cumulative amount of ATOR permeating across the rat skin was plotted against time. The study was performed in triplicate.

The permeability coefficient (*P*) of ATOR across rat skin was calculated according to Eq. (2) **(Shaker et al., 2003)**, where A is the diffusional area of the Franz cell (2.27 cm^2), C_D the concentration of ATOR in the donor chamber, and dQ/dt is the slope of the linear region of plot illustrating the amount of ATOR permeated *versus* time. Experiments were run for 24 h so that the steady state regions were around three to five times longer than the lag time.

$$P = \frac{1}{AC_D} \cdot \frac{dQ}{dt} \qquad \textbf{Eq. (2)}$$

Where, A is the diffusional area of diffusion cell, C_D is the concentration in donor chamber, dQ/dt is the slope in the steady state region of the amount of permeant.

Flux at steady state (J_{ss}) was also calculated according to the following equation:

$$J_{ss} = PC_D \qquad \textbf{Eq. (3)}$$

2.2.6. HPLC assay for quantitative ATOR determination

The ATOR concentrations were quantitatively determined by a validated analytical assay using HPLC (Shimadzu, Tokyo, Japan, equipped with Shimadzu LC-10 AD VP pump, DGU-12A degasser and SCL-10A VP system controller, Auto sampler AS4000, Photodiode array Detector). The samples of 20-µl volume were injected onto C-18 reversed-phase analytical column (Massachusetts, USA, Waters LC 2695, 10 µm particle diameter 125A, Bondpak, 4.6×250 mm). The mobile phase consisted of ortho-phosphoric acid (0.2%, v/v) and acetonitrile (80:20, v/v) in an isocratic elution mode at a flow rate of 1 mL/min. The wavelength of UV detector was set at 243 nm. No interference from any formulation components was observed during the elution of ATOR.

2.2.7. *In vivo* studies

2.2.7.1. Animals

Wistar albino rats weighing 250 ± 20 gm were supplied by the Animal house of Faculty of Pharmaceutical Sciences and Pharmaceutical Industries, Future University in Egypt (FUE). This experimental design was approved by the Research Ethics Committee of Faculty of Pharmacy, Future University in Egypt (REC-FPSPI-7/46).

2.2.7.2. PD Study design

Forty-eight Wistar albino rats were employed in the PD study. Before initiation of hypercholesterolemia, blood samples were withdrawn from the retro-orbital vein from all rats and analyzed using Liquizyme cholesterol measuring kit. After establishing the baseline cholesterol level, the rats were fed with atherogenic diet for 60 days to initiate hypercholesterolemia. The atherogenic cholesterol diet consisted of 5% hydrogenated vegetable fat, 5% butter, 1% cholesterol powder and 0.5% coconut oil, all mixed with pellet chow as reported by **(Minhajuddin et al., 2005)**, with slight modifications. The rats were divided into 8 groups, each consisted of 6 rats. The transdermal formulae; F1, F1E, F1EP, F1EL, and ATOR in OA were applied in order from G-1 to G-5. ATOR oral dispersion was administered to G-6. A negative control group that did not receive any induction or treatment and another positive control (induced, untreated) group were both included to assess the effect of atherogenic diet and treatments on plasma TC levels.

2.2.7.2.1. Blood sampling and preparation

One mL of blood was withdrawn from each rat through the retro-orbital sinus vein using heparinized glass capillary, blood samples were then left for 20 min then centrifuged at 5000 rpm at - 4°C for 5 min. Once the blood serum was separated, 10 µl-sample was then transferred carefully to a test tube which contained 1mL of measuring kit reagent. The test tube was then shaken gently and left for 10 min for the reagent to react with cholesterol in the plasma producing

a pink or purple color. It was then measured against standard using colorimetric analysis. The plasma total cholesterol (TC) was calculated *via* the following equation described by the measuring kit manufacturer.

$$\text{Plasma TC concentration} = \frac{(\text{specimen absorption})}{(\text{standard absorption})} \times 200 \quad \textbf{Eq. (4)}$$

2.2.7.2.2. Assessment of hypocholesteremic effect

After 60 days of feeding the rats on the atherogenic diet, the successful induction of hypercholesteremia was confirmed by measuring cholesterol levels with the same cholesterol measuring kit technique mentioned above. After confirming hypercholesteremia, the dorsal side of rats was shaved using electric shaver, all the rats in the groups were mildly sedated by intraperitoneal injection of Xyla-ject (20 mg/kg), to ease the application of plastic donor caps containing each formula (20 mg ATOR/ gm formula)**.** The cap reservoir was applied onto a 2 cm^2 - dorsal area using skin glue (ARcare®, Adhesives Research Inc, Pennsylvania, USA) that created a seal around the cap edges and held the cap onto the skin during the delivery time. Caps were then peeled away without causing skin damage **(Shaker et al., 2007)**.

The same application procedure was carried out for groups (G-1 to G-5), while G-6 received ATOR dispersion using oral gavage. Treatments (20 mg ATOR/gm formula) were applied/received daily for 7 successive days and the TC level of each rat in the 6 groups was analyzed compared to the initial level before treatment, and the percent reduction in TC level was then determined.

2.2.7.3. PK Study design

Eighteen Wistar albino rats, weighing 250 ± 20 gm, were fasted for 12 h with only access to water prior to the start of experiment. The rats were divided into three groups, each group comprised of 6 rats. G-I and G-II were applying F1EP and ATOR in OA, respectively, while ATOR oral dispersion was received to G-III, at a single drug dose of 80 mg/Kg. Both G-I and G-II were

prepared by mild sedation followed by shaving the dorsal side of each rat using an electric razor. Plastic donor cap was used in order to deliver one dose of each formula. The cap was applied as previously described **(Shaker et al., 2007)**. Heparinized tubes were used for collection of the blood samples at different time intervals; 2, 4, 6, 8, 12, 16, 18 and 24 h post-dosing. The blood samples were centrifuged at 4,000 rpm for 5 min and the plasma was collected in separate glass tubes to be kept frozen at -80°C until analysis using liquid chromatography-mass spectrometry/mass spectrometry (LC-MS/MS).

2.2.7.3.1. Analysis of ATOR plasma levels by LC-MS/MS assay

ATOR concentration was quantified by a HPLC method coupled with MS/MS detection for the determination of ATOR in plasma. The method was validated in accordance with the "bio-analytical method validation guidelines" method prior to analysis. Plasma samples (100 µL) were spiked with 20 µg/mL of simvastatin as internal standard which was then mixed for 1 min with 400 µL of diethyl ether: dichloromethane 7:3 (v/v), using the vortex mixer. The samples were subjected to centrifugation at 2,000 rpm for 10 min at room temperature. The supernatant was separated and injected into the LC-MS/MS system. The LC system was integrated with an Agilent 6420 triple quadruple LC/MS system, CA, USA. Inertsil ODS-3 C18 (50 mm x 4.6 mm, 5µm) was used as an analytical column. The mobile phase consisted of ammonium formate: Methanol 10:90 (% v/v) and the elution mode was isocratic, with a flow rate of 0.7 mL/min under ambient temperature. The temperature of the auto sampler (Agilent 1100 series Model G1311A, CA, USA) was kept constant at 25°C and the injection volume was 30 µL. Triple quadruple mass spectrometer, equipped with an electro spray ion source (Model G1948B, Agilent 1200 series, CA, USA) and operating in the positive ion mode, was used for detection of all of the analyzed samples and internal standard. Data analysis was performed using the Agilent MassHunter Qualitative Analysis B.05.00 (SP1).

The ATOR standard calibration curve was plotted by spiking blank rat plasma with standard stock solution of ATOR to obtain concentrations of 1, 2, 3, 5, 7, 10, 20, 30 and 60 ng/mL. The

standard curve was constructed by plotting the ratio of the drug peak area to that of the internal standard *versus* ATOR concentration. All assays were performed in triplicates. The unknown sample concentration could be calculated from the linear regression equation of the standard calibration curve.

2.2.7.3.2. Bioavailability assessment

The area under the plasma concentration–time curve (AUC_{0-24}) was calculated using the linear trapezoidal method, as described by **(Pathan and Mallikarjuna Setty, 2012)**. The PK parameters of ATOR (C_{max}, T_{max}, AUC_{0-24} and mean residence time 'MRT') were calculated using WinNonlin® software (Pharsight Co., Mountain View, CA, USA) after a single dose (80 mg/Kg) of optimized NE formula (F1EP), ATOR in OA and ATOR oral dispersion. The relative bioavailability (%) of transdermal ATOR to oral ATOR was also determined using the following equation:

$$\text{Relative bioavailability (\%)} = \frac{(AUC_{0-24} \text{ of transdermal ATOR})}{(AUC_{0-24} \text{ of oral ATOR})} \times 100 \qquad \textbf{Eq. (5)}$$

2.2.8. Statistical analysis

All the results were represented as mean values ± SD. Statistical analysis for PK parameters were calculated by applying two way analysis of variance (ANOVA) followed by post-hoc test using SPSS® software (IBM 20, USA).

3. Results and discussion

3.1. Selection of NE oil phase based on solubility study

Solubility of drug in excipients has a significant impact on the stability of formulae. Therefore, screening of the appropriate oil is a primary requirement of NE development. NEs should be isotropic, monophasic and must have good solubilizing capacity to incorporate single dose of drug in minimum volume of formulation.

ATOR is a hydrophobic drug with a low aqueous solubility of 1.23 mg/mL. Solubility in different oils was determined and found to be arranged as follows; oleic acid (OA) [10.34 mg/mL] > Captex® [4.23 mg/mL] > cotton seed oil [3.41 mg/mL] > sunflower oil [2.21 mg/mL]. The results obtained confirm a substantial solubilization effect of OA compared to the other oils as a result of HLB values; 1, 6, and 7 for OA (**Du et al., 2010**), cottonseed oil (**Hannan, 2007**) and sunflower oil (**Cornier et al., 2019**), respectively.

Higher oil solubility of a hydrophobic drug will favor an overall stability of the formulation. The natural long-chain fatty acid OA, which can be described as an amphiphilic compound with surfactant characteristics, is efficiently replacing the regular medium-chain triglyceride lipids, as Captex®, in the NE formulae **(Kogan and Garti, 2006)**. Therefore, OA was chosen as the oil phase owing to the higher solubility of drug in oil which leads to lower requirement of surfactant and co-surfactants, and consequently minimizes the toxic effect of surfactants. On the other hand, the high drug solubility in oil was reported to lessen the contribution of surfactant or co-surfactant in drug solubilization, hence reduce the risk of precipitation **(Shafaat et al., 2013).**

3.2. Construction of pseudo-ternary phase diagrams

On account of the results of solubility study, OA was the chosen oily phase. Tween 80/PEG 400 and Tween 20/PEG 400 were the surfactant and co-surfactant combinations selected for development of o/w NEs in this work. It was reported that the surfactants selected for o/w NEs should have HLB value greater than 10 for immediate formation of o/w droplets **(Kadu et al., 2011)**, this matches well with Tween 80 (HLB = 15) and Tween 20 (HLB = 16.7). Tweens have been shown to produce droplets with smaller sizes than those obtained from other surfactants (poloxamer 407, Span 80, etc.) **(Khayata et al., 2012)**. Furthermore, the addition of co-surfactant is mandatory as it reduces the bending stress of the interface and provides suitable flexibility to the interfacial film to adopt different curvatures necessary to form NE of small droplet sizes.

Both surfactant and co-surfactant (Smix) were mixed at different ratios, hence five pseudo-ternary phase diagrams were designed and presented in **Fig. 1(A-E)**, respectively. The investigations of the phase diagrams help to select the appropriate concentration of excipients, i.e., oil proportion and optimum Smix ratio aiming to produce NE with good stability **(Ali and Hussein, 2017)**. The shaded region indicates NE region, a wider region indicates a better and a more stable NE system. It is worth to clarify that the formulae prepared with Tween 80/PEG 400 (Smix 3:1) were physically unstable upon preparation and thus were not included in further studies.

It is observed that system I containing Tween 80 showed the widest NE regions compared to system III containing Tween 20 at the same Smix ratio. Although the HLB values of the incorporated surfactants are higher than 10, there was a significant variation in their capability to emulsify oils. The results obtained indicated that in addition to HLB value, there are other factors like structure and relative length of hydrophobic chains of surfactants that affect the creation of NE. The fact could be ascribed to the longer unsaturated fatty acid chains (C18) of Tween 80 than that of Tween 20 (saturated C12 chains), imparting more flexibility in the structure of the former, and hence better emulsification potential.

The NE formation is thermodynamically spontaneous, due to the presence of surfactant which reduces the interfacial tension, hence lowering the free energy required to form an emulsion. All of the NEs formed were stable which could be the result of higher HLB value of Tweens, and higher solubilizing capacity of PEG 400. Furthermore, surfactants supply mechanical barrier to coalescence **(Resende et al., 2008)**. A narrow NE area was observed in case of Smix 2:1 and 3:1 **[Fig. 1(B, D** and **E)]** in comparison to Smix 1:1 **[Fig.1 (A** and **C)]**. That is to say increasing co-surfactant proportion induces NE formation and stability. The fact may be accredited to the water miscibility of PEG and its affinity to redistribute itself between the aqueous phase and emulsion–water interface, hence reducing co-surfactant content leads to loss of solvent capacity which results in an unstable emulsion. These results indicated that the quantity

of PEG 400 was directly proportional to emulsion stability which was in accordance with previous reports **(Ibrahim et al., 2016)**. The addition of PEG 400, particularly when combined with Tween 80, provided further reduction in the surface tension and fluidized the interfacial surfactant film which can expand the area of formation of NE system **(El Maghraby, 2008)**. Therefore, different NE formulae were selected based on the pseudo-ternary diagrams drawn, the composition of these NE formulations are collected in **Table 1**.

3.3. Characterization of the selected ATOR-loaded NEs

The chosen formulations were loaded with ATOR at a concentration of 20 mg/g NE. The drug completely dissolved without any signs of precipitation observed. NEs were found stable upon storage at room temperature for three months.

3.3.1. Measurement of Droplet size, polydispersity index (PDI) and zeta potential (ZP)

The droplet size, PDI and ZP were measured for the selected NE formulae after being loaded with ATOR at a concentration of 20 mg/g NE, and the results are demonstrated in **Table 2**.The droplet size of the NE is an essential factor on account of its significance in determination of the extent and rate of the release of the drug leading to penetration improvement **(Khurana *et al*., 2013)**. The results showed that the droplet sizes ranged from 111.8 ± 16.6 to 195.6 ± 14.3 nm, demonstrating all experimental formulae were in NE range. Increasing Smix content revealed a negligible effect on droplet size. As obvious, the formulae containing about 80% w/w Smix showed the smallest droplet size, this observation was in agreement with Kallakunta et *al.* who stated that minimum droplet size was observed between 70 and 80% of surfactant system concentration. They attributed their finding to rapid formation of the droplets with higher surfactant/oil ratio **(Kallakunta et al., 2012)**. Another explanation is the stabilization of o/w interface and formation of a better closed pack film, leading to fast arrangement of the droplets which subsequently results in smaller droplet size (**Balata et al., 2016)**. Small droplets have a

greater liability to be attached to membranes, as well as transporting drug in a further controlled way and covering a wide surface area, **(Kogan and Garti, 2006)**.

The PDI results ranged from 0.17 to 0.62. Only NE formulae with PDI < 0.3 were selected indicating a narrow deviation of average size and homogenous population. Also, the ZP of all ATOR NEs prepared were in the range of −15 to −30 mV. These negative charges could be attributed to the presence of the polyethoxylate ion in both Tween 80 and Tween 20, which forms hydrogen bonds with the continuous phase water molecules in the boundary layer of o/w NE **(Nursakinah et al., 2015)**. Based on the previous results, formulae F2, F4, F5 and F7 contained a Smix ratio less than 80% w/w that ranges from 45-60% w/w were excluded from further studies, while formulae F1, F3, F6, F8 and F10 were selected for further investigations.

3.3.2. *In vitro* ATOR release studies

For the *in vitro* drug delivery evaluation, the study was carried out to analyze drug release from the selected five NE formulae F1, F3, F6, F8 and F10. The experiment was conducted through cellulose membrane using PBS pH 7.4 containing 10% methanol as receptor solution. The release data are illustrated in **Fig. 2**. The release rate was the fastest in F1 but the slowest in F3. The percentages of ATOR released after 8 h from the prepared formulae could be arranged in descending order as follows: F1=F8>F6>F10>F3, with release percentage of 100, 100, 92.9, 72.9 and 48.2%, respectively. These results could be ascribed to the small droplet size range (111.8-168.2 nm) of all formulae under study except F3 which acquired the largest size (241.3 nm). The significant higher droplet size (p<0.05) of F3, compared to other formulae, could be the main reason for its sustained release profile. However, it was observed that the variation of droplet size within the tested range (111.8-168.2 nm) does not appear to have any major influence on drug release, hence no clear relation could be established between NE droplet size and the release profiles.

The results indicated that F1 reached complete drug release after 6 h with a release efficiency of 61% followed by F8 after 8 h attaining 49.3% efficiency. This could be ascribed to the influential effect of Tween 80 on ATOR solubilization capacity in the former formula compared to Tween 20 in the latter one. Therefore, F1 and F8 were chosen for further optimization.

3.4. Optimization of the selected ATOR-loaded NEs

On the basis of *in vitro* study data, F1 and F8 were selected for further optimization by the incorporation of ethanol and D-limonene as penetration enhancers at different concentrations. F1, composed of 9% OA, 40.5% Tween 80, 40.5% PEG 400 and 10% water, was optimized by different ways; ethanol, being a co-surfactant with penetration enhancement property, was entirely replacing PEG 400 forming formula F1E (9% OA, 40.5% Tween 80, 40.5% Ethanol and 10% water). In another trial, ethanol was included by replacing half-proportion of PEG 400 developing formula F1EP with the following composition: 9% OA, 40.5%Tween 80, 20% PEG 400, 20.5% Ethanol and 10% water. Acting as an effective penetration enhancer, D-limonene was incorporated at 5% concentration in conjunction with ethanol and PEG 400 preparing formula F1LEP with the following constituents: 9% OA, 40.5% Tween 80, 10% PEG 400, 25.5% Ethanol, 5% Limonene, and 10% water. The concentration of D-limonene was adjusted at 5% (w/w), considered to be the optimum concentration to enhance the transdermal flux, and above which a decrease in penetration profile occurs as reported by **(Chandrashekar and Hiremath, 2008)**. Also, 5% D-limonene (w/w) could be tolerable as it did not show any skin erythema and edema after application on rabbit skin as described by **(Lakshmi, 2014)**. Accordingly, both ethanol and limonene were tried to be included in F8, constituting of 9% OA, 53.5%Tween 20, 27.5% PEG 400 and 10% water, however the addition of any penetration enhancers resulted in instability of the formula. This result was in accordance with Tadros *et al* who reported that Tween 20 as surfactant can lead to lower NE stability being more susceptible to surface area fluctuations, increasing creaming and coalescence phenomena **(Tadros, 2013)**.

3.5. Characterization of the optimized ATOR-loaded NEs

3.5.1. Droplet size, PDI and ZP

The droplet size, PDI and ZP of the optimized NE formulae were detected (**Table 2)**. The mean size ranged from 142.5 to 320.2 nm confirming that all prepared NEs are sub-micron emulsions. Surprisingly, larger droplet sizes were significantly formed in all optimized formulae containing ethanol (p<0.05) when compared to F1. This might be attributed to the dilution performed during particle size measurement, mostly affecting alcohol containing NE, which may lead to a disordering at the interfacial film stabilizing the oil droplets, and hence coalescence. The PDI was in the range of 0.19 to 0.41, indicating a limited size distribution. All formulae showed a relatively high surface charge ranging from -13 to -26.3 mV, confirming good system stability.

3.5.2. Morphology imaging using TEM

TEM is considered one of the most crucial approaches applied to visualize NE droplets morphology. TEM images of the optimized NE formulae are illustrated in **Fig. 3**. The NE droplets occur as dark spheres and the surroundings were of bright color. The droplets were seen as nanometer-sized spherical particles, without visible drug crystals which confirm the good state of NE. The formula F1 showed a droplet size ranging from 18.99 to 23.73 nm, while F8 from 23.45 to 47.7 nm. To confirm the morphology of the formulae after the inclusion of penetration enhancers, both F1E and F1EP were imaged using TEM and illustrated in **Fig. 3**. F1E and F1EP displayed droplet nano-sizes ranging from 43.32 nm to 88.99 nm and from 17.86 nm to 36.21 nm, respectively.

The droplet size range determined by TEM was significantly smaller than that obtained by dynamic light scattering technique. This may be ascribed to the drying process applied for NE samples before measurement, in addition to the dehydration caused by the vacuum system in TEM imaging chamber **(Klang et al., 2013).**

3.5.3. Viscosity determination

As shown in **Table 2**, both formula F1 and F8 exhibited the highest viscosities, compared to the other formulae. This can be accredited to the presence of PEG 400 in both formulae **(El Maghraby, 2008)** There was no significance difference between the viscosity of F1EP and F1LEP ($p > 0.05$), but their viscosities were significantly higher than F1E ($p < 0.05$). This could be the result of the high ethanol concentration in the latter formula.

3.6. *Ex vivo* skin permeation study

The skin permeation of all optimized ATOR-loaded NE formulations were studied, and compared to ATOR solubilized in OA. The reason we choose to study *ex vivo* and *in vivo* skin permeation of ATOR from NE and comparing it to drug in OA is to challenge the belief that NE, as a dosage form is by default enhances the release of drugs through the skin, since OA is a permeation enhancer that causes the SC to swell due to more water absorption. OA also compromises some of the basic elements of the SC, hence deepening permeation through this limiting and protective barrier **(Kogan and Garti, 2006).** Skin permeation profiles of ATOR from different formulae across rat skin at different time intervals are illustrated in **Fig. 4**. As obvious, F1EP exhibited the highest cumulative ATOR permeated, while F1, F8 and ATOR in OA were the least. The permeation parameters were also calculated and are presented in **Fig. 5**. The permeability coefficient (*P*) is a quantitative measure of the rate at which the drug molecule can cross a membrane, expressed in cm/h, however the flux (*Jss*) measures the amount of solute diffusing a cross-sectional area of the membrane over time, expressed in μg/cm^2/h. By observing the results of both parameters, the various formulations can be arranged based on the rate and extent of drug permeation in a descending manner as follows: F1EP > F1LEP > F1E > F1 > ATOR in OA > F8. Although its high solubilization capacity as well as its inherent penetration enhancement effect, OA alone failed to enhance ATOR permeation across rat skin with a *P* and Jss values of 6.9 cm/h and 1.38 μg/cm^2/h, respectively. Indeed, the statistical analysis revealed no significant difference (p<0.05) between drug fluxes obtained in case of ATOR in OA, F1 and

F8, indicating that o/w NE without any penetration enhancers had negligible effect on isolated skin permeation testing. The effect of both skin hydration and nanosizing associated with o/w NEs had actually minimal effect on ATOR transdermal permeation. The follicular delivery also could be assumed not being the pathway for permeation of ATOR NEs, since skin follicles tend to collapse *in vitro* and *ex vivo*, as they are blocked with dry sebum and secretions, thus become inactive **(Verma *et al*., 2016)**. The high viscosity of these formulations (**Table 2**), hence the low thermodynamic activity of the drug could be the reason for such retardation in ATOR permeation.

The addition of ethanol in F1E improved ATOR flux through rat skin by 6 folds reaching 53 cm/h and 10 µg/cm^2/h for *P* and Jss, respectively, when compared to F1. Ethanol acts as a hydrotrope which adequately reduces the interfacial tension of surfactant film located between the oily and aqueous phases, exerting a clear impact on both the density and viscosity of the NE **(Tenjarla, 1999).** Also, ethanol has the capability to reversibly alter the SC and increase permeation through boosting fluidity in the transport rate-limiting lipid regions **(Kouchak and Handali, 2014).** Ethanol penetrates the skin and fluidizes significant amounts of the lipid barrier material from the SC. This lipid fluidization could lessen the function of skin barrier and provide more permeability to the membrane, which is the most likely explanation for the effect of ethanol as a skin penetration enhancer **(Van der Merwe and Riviere, 2005).** The influence of ethanol as a skin penetration enhancer was expressed as a 'pull' or 'drag' effect promoting solute penetration **(Lachenmeier, 2008).**

The maximum drug flux was observed in case of F1EP, attaining 98 cm/h and 19.6 µg/cm^2/h of *P* and *Jss*, respectively, which was higher than that obtained from F1E. Lower ethanol concentration in F1EP (20.5%) was found more efficient in fluidizing the SC lipid bilayer, when compared to 40% ethanol in F1E. These results agree with those obtained by **(Sakdiset *et al*., 2017)**, where moderate concentration of ethanol resulted in enhancement of the permeant flux, while further increase of ethanol resulted in reduction of this flux**.** The augmenting effect of ethanol seems to have an ideal range **(Pershing *et al*., 1990)** where dehydration of the skin

membrane occurs at highly concentrated ethanol and thus, reducing the drug permeation through it **(Williams and Barry, 2012).**

Moreover, the flux results achieved by F1EP could be attributed to the additional interaction of PEG 400 with the intercellular lipids causing a disruption in their organization and an increase in their fluidity, and also partly as a result of solubilization of lipid bilayers by PEG 400, as reported by **(Shah *et al*., 2013).** Moreover, the synergistic effect exerted when PEG 400 was associated with ethanol regarding penetrating enhancing potential facilitated ATOR permeation. A previous study reported the synergistic effect of multiple components to enhance skin penetration **(Karande and Mitragotri, 2009).** The synergistic enhancements obtained from a mixture of propylene glycol and alcohols have been documented by **(Kaiho *et al*., 1989).**

On the other hand, F1 showed lower skin permeation compared to F1EP, although the higher proportion of PEG 400 in the former formulation than the latter (40.5% *versus* 20% PEG 400, respectively). The fact could not be ascribed to the solubilization capacity of PEG 400, but to the reduction in drug thermodynamic activity based on the high viscosity of F1 (309 cPs), as interpreted before. This result was in agreement with the findings confirming no correlation between drug solubilizing effect and permeation **(Hamishehkar *et al*., 2015).**

However, reducing PEG 400 concentration below 20% in case of F1LEP (10% PEG 400 along with 25.5% ethanol and 5% limonene), compared to F1EP seems to have a lowering penetration enhancing effect even with the addition of 5% limonene, where the respective *P* and Jss values were 54 cm/h and 10.9 µg/cm^2/h**.** However, the addition of limonene in F1LEP did not enhance the permeation of ATOR, comparable to F1E. These results went parallel with that reported by **(Almirall *et al*., 1996)**, where limonene even reduced the transdermal permeability.

The overall permeation pattern can be expressed according to the following equation (**Shaker et al., 2003)**:

$$P_{SC} = P_L + P_P \qquad \textbf{Eq. (6)}$$

where P_{SC} is the permeability coefficient of the SC, P_L and Pp are the permeability coefficients for the lipoidal and pore (follicular) pathways, respectively.

Therefore, the *ex vivo* permeation experiments suggest that the lipoidal pathway (P_L) dominates for the hydrophobic permeant ATOR as a result of the collapse of skin follicles. The driving force is fluidization of phospholipid bilayer by penetration enhancers and other NE components. Thus, the total permeability coefficient can be expressed by the following model:

$$P_{SC} \approx P_L \qquad \textbf{Eq. (7)}$$

However, during *in vivo* studies, the follicular delivery (pore pathway P_P) could not be neglected due to the existence of open skin follicles. Therefore, the *in vivo* studies are mandatory for investigating the permeation pathways of lipophilic permeants like ATOR and confirming the importance of NEs in their transdermal permeation.

3.7. *In vivo* studies

3.7.1. PD results

3.7.1.1. Induction of hypercholesterolemia in rats

After 60 days of feeding rats on atherogenic diet, blood samples were collected, and plasma TC levels were measured using Liquizyme measuring kit. The mean plasma TC level of all rats under study had an average of 156.5 mg/dL after induction in comparison to the initial mean data (95.9 mg/dL), indicating an elevation by 63%. The negative control (non-induced) group showed non-significant change in its TC level (p>0.05) after the induction period measuring 98.3 ± 6.1 mg/dL, compared to its initial measurement (96.1 ± 4.2 mg/dL). The hypercholesteremia was then successfully induced in rats due to the atherogenic feed as previously reported in earlier study **(Dietschy et al., 1993)**.

3.7.1.2. Assessment of hypocholesteremic effect

The selected NE formulae and ATOR in OA were applied on the shaved dorsal side of the rats' skin, as illustrated in Supplementary Figure and described before. No signs of erythema or irritation were observed at the site of application during the treatment period. The mean plasma TC levels before (baseline) and after 7 successive days of receiving the treatments in hypercholesterolemic rats are collected in **Table 3**. The administration of all treatments significantly decreased the mean plasma TC level ($p<0.05$). The % reduction of plasma TC level in all groups ranged from 11.4 to 27.2%, where F1EP showed the highest decrease in TC, followed by F1E, F1LEP then F1. A non-significant difference in percent reduction of TC levels was found between groups 1, 2 and 4 ($p>0.05$), all NE formulae showed a higher % reduction than drug in OA, this could be attributed to NE ability to retain the drug within skin layers. Data revealed the superiority of F1EP over other NE formulae in enhancing ATOR transdermal permeation, hence improving the disease condition. These results were in agreement with flux data of *ex vivo* skin permeation experiments discussed earlier.

On the other hand, ATOR oral dispersion exhibited higher hypocholesteremic effect, compared to ATOR in OA. This result may be partially attributed to ATOR active metabolites (para-hydroxy and ortho-hydroxy-ATOR) metabolized principally in the liver by the cytochrome P450 system. These metabolites further extend HMG-CoA reductase inhibition by up to 30 h, a property that contributes to the drug greater efficacy for lowering blood cholesterol, compared to other statins **(Williams and Feely, 2002).**

As obvious, all NE formulae showed higher hypocholesteremic effect than ATOR oral dispersion ($p<0.05$). This could be elucidated by the enhanced bioavailability of ATOR by transdermal delivery, ascribed to the enhanced NE permeation due to their nano-sized oil droplets, in addition to NE components which cause a disruption in SC lipid bilayer **(Shaker et al., 2019)**.

The study demonstrated the effectiveness of transdermal ATOR NE in reducing hyperlipidemia by direct drug delivery to the circulation, assuming a reduction of the metabolic load on liver, hence non-elevation in the activity of liver enzymes, due to avoidance of first-pass

metabolism. The results of PD study confirm the superiority of FIEP NE formula, therefore it was selected for further PK study in comparison to the oral dispersion and ATOR in OA as well.

3.7.2. PK results

3.7.2.1. Quantitative ATOR determination in plasma using LC-MS/MS.

The adopted analytical assay was validated in terms of accuracy, precision, linearity and specificity. The peak areas of ATOR serial concentrations were determined and the ratio between each ATOR peak area relative to that of the internal standard (simvastatin) was deduced and plotted against ATOR concentration. A linearity was confirmed over the selected concentrations with a correlation coefficient (R^2) of 0.9979. The linear regression equation of the standard calibration curve was y = 0.0158 x + 0.0104, where y is the peak area ratio and x is ATOR concentration in (ng/mL).

3.7.2.2 PK parameters and bioavailability assessment

The optimized transdermal NE (F1EP) was chosen for bioavailability assessment being the highest in terms of drug permeation extent across rat skin and % reduction in plasma TC level as well, compared to the other NE formulae. The plasma drug concentration-time curves for different formulae under study are illustrated in **Fig. 6** and the PK parameters are presented in **Table 4**.

Compared to the other formulae under study, F1EP exhibited the lowest C_{max} with a delayed T_{max}. These results might be ascribed to the skin retention of NE associated with a slow partitioning of the drug into the skin as reported in literature **(Shaker et al., 2019)**.

ATOR oral dispersion resulted in a higher C_{max} than that of NE but with a short T_{max}. The fact could be attributed due to the rapid absorption followed by drug metabolism in the liver by first-pass effect as previously clarified. Similar results were reported for oral administration of carvedilol, which reached C_{max} after 2 h, while its transdermal NE gel resulted in C_{max} that was

reached after 12 h **(Pratap et al., 2012)**. Both ATOR oral dispersion and ATOR in OA showed almost comparable C_{max} and T_{max} parameters.

On the other hand, ATOR NE exhibited a significant higher bioavailability (p<0.05), expressed by 2-fold increase in AUC_{0-24} value, than the other formulae under study. This was due to the depot action of transdermal NE which offers a means for sustainment in drug release. The oral ATOR dispersion showed a rapid elimination from the plasma as indicated by significantly lower values of AUC_{0-24} compared to ATOR NE (p<0.05). This result was in agreement with the PK parameters of Olmesartan transdermal NE which revealed a greater extent of permeation compared to the oral dose **(Aqil et al., 2016).** Vinpocetine also showed higher bioavailability when released from transdermal NE when compared to commercial oral tablets **(El-Laithy et al., 2011)**. In another study, transdermal application of theophylline ME showed increased AUC by 1.65-fold higher than that of the oral administration of theophylline tablets in rabbits **(Zhao et al., 2006)**

A non-significant difference in AUC_{0-24} was found between ATOR in OA and ATOR oral dispersion (p>0.05). This result confirms the incapability of ATOR in OA to effectively enhance the transdermal delivery of the lipophilic drug.

Accordingly, the relative bioavailability of ATOR NE was found higher by two folds than the oily drug solution which only showed a 12% increase in its systemic availability compared to oral dispersion. This indicates an extended drug existence in the plasma in case of NE formula, also confirmed by a higher MRT value of 11.3 h and could be ascribed to the deposition of ATOR NE within the skin layers, which in turn serves as a drug reservoir for extended release into the viable epidermis over hours **(Benigni et al., 2018).**

Transdermal NE was proved to be more efficient in delivering ATOR to the systemic circulation compared to oral dispersion and ATOR in OA as well. However, the *in vivo* results obtained in this work seem not well correlated to the *ex vivo* findings. F1EP showed the steepest *ex vivo* permeation profile compared to ATOR in OA, while the same NE formula exhibited the most

sustained drug release *in vivo*. The result could be explained by the collapse of hair follicles during *ex vivo* skin permeation study. The NE formula was thus forced to only pass through the lipoidal pathway which accelerated the transport of the drug based on the effect of NE components (ethanol and PEG 400) in disrupting SC lipids. Therefore, modifying the NE permeation pathway towards the appendageal route, specifically *via* follicular delivery, may have contributed to deliver ATOR *in vivo* in a more controlled and sustained manner. Such pathway is not applicable when the drug is delivered from the oil. In addition, the cessation of perifollicular circulation as proposed by **Verma et al., 2016** might cause the variation between *ex vivo* and *in vivo* results.

4. Conclusion

The present work developed ATOR-loaded NE for transdermal delivery aiming to avoid its extensive portal circulation, increase its bioavailability and hence improve its therapeutic effect. The NE formulations were prepared using OA, Tween 80 or Tween 20, and PEG 400 as oil, surfactant and co-surfactant, respectively. The medicated NEs containing 20 mg ATOR/g formula exhibited nano-sized spherical droplets with homogenous distributions and negative surface charges. The integration of ethanol as PE at a concentration of 20.5% (w/v) in F1EP significantly improved the drug flux through full-thickness rat skin reaching 19.6 µg/cm^2/h and 98 cm/h for *Jss* and *P*, respectively. The optimized ATOR-loaded NEs were assessed *in vivo* for their hypocholesteremic effect as well as systemic availability in comparison to ATOR oral dispersion and ATOR in OA. F1EP showed the highest decrease in TC level by 27%, and a significant higher relative bioavailability of 214.3% with a lower C_{max} but an extended plasma profile. The study revealed a non-correlation between *ex vivo* and *in vivo* results suggesting that *in vivo* experimentation may be a more accurate indication when both lipoidal and appendageal pathways were expected. The *ex vivo* studies are good predictable tools when the follicular pathway can be neglected for transdermal drug delivery. Further confirmatory investigations are in progress endorsing the drug transdermal pathways and the potential mechanisms by which NE enhanced ATOR permeation through the skin. It would be possible to develop a wrist strap time-controlled

device that carries drug loaded NE. The device will allow drug delivery for a certain period of time during the day without having the patient worry about oral dosing schedule around feeding hours and gastric side effects.

References

Adams, S.P., Tsang, M., Wright, J.M., 2015. Atorvastatin for lowering lipids. Cochrane Database Syst. Rev. 3, 1-24.

Ali, H.H., Hussein, A.A., 2017. Oral nanoemulsions of candesartan cilexetil: formulation, characterization and in vitro drug release studies. AAPS Open.3, 1-16. https://doi.org/10.1186/s41120-017-0016-7

Almirall, M., Montaña, J., Escribano, E., Obach, R., Berrozpe, J.D., 1996. Effect of d-limonene, alpha-pinene and cineole on in vitro transdermal human skin penetration of chlorpromazine and haloperidol. Arzneimittelforschung. 46, 676–80.

Aqil, M., Kamran, M., Ahad, A., Imam, S.S., 2016. Development of clove oil based nanoemulsion of olmesartan for transdermal delivery: Box–Behnken design optimization and pharmacokinetic evaluation. J. Mol. Liq. 214, 238–248. https://doi.org/10.1016/J.MOLLIQ.2015.12.077

Balata, G. F., Essa, E. A., Shamardl, H. A., Zaidan, S. H., Abourehab, M. A. 2016. Self-emulsifying drug delivery systems as a tool to improve solubility and bioavailability of resveratrol. Drug Des. Devel. Ther.10, 117–128. doi:10.2147/DDDT.S95905

Bhagya, R., 2018. Formulation and Characterization of Atorvastatin Ethosomal Gel. J. Drug Dev. Del.1, 13–20.

Bhatt, P., Madhav, S., 2011. A detailed review on nanoemulsion drug delivery system. Int. J. Pharm. Sci. Res. 2, 2292–2298.

Chandrashekar, N.S., Hiremath, S.R.R., 2008. In vivo Immunomodulatory, Cumulative Skin Irritation, Sensitization and Effect of d-Limonene on Permeation of 6-Mercaptopurine through Transdermal Drug Delivery. Biol. Pharm. Bull. 31, 656–661. https://doi.org/10.1248/bpb.31.656

Chavhan, S.S., Petkar, K.C., Sawant, K.K., 2013. Simvastatin nanoemulsion for improved oral delivery: Design, characterisation, in vitro and in vivo studies. J. Microencapsul. 30, 771–779. https://doi.org/10.3109/02652048.2013.788085

Chojnacki C, Błońska A, Chojnacki J., 2017. The Effects of Melatonin on Elevated Liver Enzymes during Statin Treatment. Biomed Res Int.2017, 3204504. doi:10.1155/2017/3204504).

Çinar, K., 2017. A Review on Nanoemulsions: Preparation Methods and Stability. Trak. Univ. J. Eng. Sci. 18, 73–83.

Cornier, J., Keck, C.M., Van de Voorde, M. 2019. Nanocosmetics From Ideas to Products, first ed. Springer Nature, Switzerland.

Davies, J.T., Delfino, S.F., Feinberg, C.E., Johnson, M.F., Nappi, V.L., Olinger, J.T., Schwab, A.P., Swanson, H.I., 2016. Current and Emerging Uses of Statins in Clinical Therapeutics: A Review. Lipid Insights 9, 13–29. https://doi.org/10.4137/LPI.S37450

Dietschy, J.M., Turley, S.D., Spady, D.K., 1993. Role of liver in the maintenance of cholesterol and low density lipoprotein homeostasis in different animal species, including humans. J. Lipid Res. 34, 1637–1659.

Doherty, M.M., Pang, K.S., 1997. First-Pass Effect: Significance of the Intestine for Absorption and Metabolism. Drug Chem. Toxicol. 20, 329–344. https://doi.org/10.3109/01480549709003891

Du, C. B., Chen, W. Q., and Wan, F. X., 2010. Influence of HLB Parameters of Surfactants on Properties of Magneto-Rheological Fluid. Adv. Mater. Res. 97–101, 843–847. https://doi.org/10.4028/www.scientific.net/amr.97-101.843

El Maghraby, G.M., 2008. Transdermal delivery of hydrocortisone from eucalyptus oil microemulsion : Effects of cosurfactants. Int. J. Pharm. 355, 285–292. https://doi.org/10.1016/j.ijpharm.2007.12.022

El-Laithy, H.M., Shoukry, O., Mahran, L.G. 2011. Novel sugar esters proniosomes for transdermal delivery of vinpocetine: preclinical and clinical studies. Eur. J. Pharm. Biopharm. 77, 43-55.

Fessi, H., 2012. Preparation of vitamin E loaded nanocapsules by the nanoprecipitation method: From laboratory scale to large scale using a membrane contactor. Int. J. Pharm. 423, 419–27.

Hamishehkar, H., Khoshbakht, M., Jouyban, A., Ghanbarzadeh, S., 2015. The Relationship between Solubility and Transdermal Absorption of Tadalafil. Adv. Pharm. Bull. 5, 411–417. https://doi.org/10.15171/apb.2015.056

Hannan, H.J. Technician's Formulation Handbook for Industrial and Household Cleaning Products. 2007. Waukesha, Wisc. Kyral LLC, USA

Ibrahim, N., Raman, I.A., Yusop, M.R., Sis, H., Birinci, M., Ita, B.I., Iweala, E.E.J., Chemistry, A., 2016. the Effect of Polyethylene Glycol (PEG) Coating on the Magneto-Structural Properties and Colloidal Stability of 11, 7–14. https://doi.org/10.1016/j.colsurfa.2009.03.039

Kadu, P.J., Kushare, S.S., Thacker, D.D., Gattani, S.G., 2011. Enhancement of oral bioavailability of atorvastatin calcium by self-emulsifying drug delivery systems (SEDDS). Pharm. Dev & tech 16, 65–74. https://doi.org/10.3109/10837450903499333

Kaiho, F., Koike, R., Nomura, H., Hara, H., Maruoka, K., Dohi, M., Kato, Y., 1989. Enhancing effect of cetyl lactate on the percutaneous absorption of indomethacin in rats. Chem. Pharm. Bull. (Tokyo). 37, 1114–1116. https://doi.org/10.1248/cpb.37.1114

Kallakunta, V.R., Bandari, S., Jukanti, R., Veerareddy, P.R., 2012. Oral self emulsifying powder of lercanidipine hydrochloride: Formulation and evaluation. Powder Technol. 221, 375–382. https://doi.org/10.1016/J.POWTEC.2012.01.032

Karande, P., Mitragotri, S., 2009. Enhancement of transdermal drug delivery via synergistic action of chemicals. Biochim. Biophys. Acta - Biomembr. 1788, 2362–2373. https://doi.org/10.1016/J.BBAMEM.2009.08.015

Khayata, N., Abdelwahed,W., Chehna, M.F., Charcosset, C., Fessi, H., 2012. Preparation of vitamin E loaded nanocapsules by the nanoprecipitation method: From laboratory scale to large scale using a membrane contactor. Int. J. Pharm. 423, 419–27.

Khurana, S., Jain, N.K., Bedi, P.M.S., 2013. Nanoemulsion based gel for transdermal delivery of meloxicam: Physico-chemical, mechanistic investigation. Life Sci. 92, 383–392. https://doi.org/10.1016/j.lfs.2013.01.005

Klang, V., Valenta, C., Matsko, N.B., 2013. Electron microscopy of pharmaceutical systems. Micron 44, 45–74. https://doi.org/10.1016/j.micron.2012.07.008

Kogan, A., Garti, N., 2006. Microemulsions as transdermal drug delivery vehicles. Adv. Colloid Interface Sci. 123–126, 369–385. https://doi.org/10.1016/j.cis.2006.05.014

Kouchak, M., Handali, S., 2014. Effects of Various Penetration Enhancers on Penetration of Aminophylline Through Shed Snake Skin. Jundishapur J. Nat. Pharm. Prod. 9, 24–29. https://doi.org/10.17795/jjnpp-12904

Lachenmeier, D.W., 2008. Safety evaluation of topical applications of ethanol on the skin and inside the oral cavity. J. Occup. Med. Toxicol. 3, 26. https://doi.org/10.1186/1745-6673-3-26

Lakshmi, P.K., Mounika, K. and Saroja, C.H., 2014. Transdermal Permeation Enhancement of Lamotrigine Using Terpenes. Pharm. Care Heal. Syst. 1, 1–6. https://doi.org/10.4172/jpchs.1000103

Mahmoud, M.O., Aboud, H.M., Hassan, A.H., Ali, A.A., Johnston, T.P., 2017. Transdermal delivery of atorvastatin calcium from novel nanovesicular systems using polyethylene glycol fatty acid esters: Ameliorated effect without liver toxicity in poloxamer 407-induced hyperlipidemic rats. J. Control. Release. 254, 10–22. https://doi.org/10.1016/j.jconrel.2017.03.039

Minhajuddin, M., Beg, Z.H., Iqbal, J., 2005. Hypolipidemic and antioxidant properties of tocotrienol rich fraction isolated from rice bran oil in experimentally induced hyperlipidemic rats. Food Chem. Toxicol. 43, 747–753. https://doi.org/10.1016/J.FCT.2005.01.015

Nursakinah, I., Ismail Ab Raman1, Muhammad Rahimi Yusop, 2015. Effects of functional group of non-ionic surfactants on the stability of emulsion. Malaysian J. Anal. Sci. 19, 261–267.

Pathan, I.B., Mallikarjuna Setty, C., 2012. Nanoemulsion system for transdermal delivery of tamoxifen citrate: Design, Characterization, effect of penetration enhancers and in vivo studies. Dig. J. Nanomater. Biostructures. 7, 1373–1387.

Pershing, L.K., Lambert, L.D., Knutson, K., 1990. Mechanism of ethanol-enhanced estradiol permeation across human skin in vivo. Pharm. Res. 7, 170–5.

Pratap, S.B., Brajesh, K., Jain, S.K., Kausar, S., 2012. Development and Characterization of A Nanoemulsion Gel formulation for Transdermal delivery of Carvedilol for Transdermal delivery of Carvedilol. Int. J. Drug Dev. & Res. 4, 151–161.

Ramadan, A.A., Mandil, H., Sabouni, J., 2015. Determination of atorvastatin calcium in pure and its pharmaceutical formulations using iodine in acetonitrile by UV-visible spectrophotometric method. Int. J. Pharm. Pharm. Sci. 7, 427–433.

Resende, K.X., Corrêa, M.A., Gomes De Oliveira, A., Scarpa, M.V., Scarpa, M. V, 2008. Effect of cosurfactant on the supramolecular structure and physicochemical properties of non-ionic biocompatible microemulsions. Brazilian J. Pharm. Sci. 44, 35–42. https://doi.org/10.1590/S1516-93322008000100005

Rodde, M.S., Divase, G.T., Devkar, T.B., Tekade, A.R., 2014. Solubility and bioavailability enhancement of poorly aqueous soluble atorvastatin: in vitro, ex vivo, and in vivo studies. Biomed. Res. Int. 2014, 463895. https://doi.org/10.1155/2014/463895

Sakdiset, P., Kitao, Y., Todo, H., Sugibayashi, K., 2017. High-Throughput Screening of Potential Skin Penetration-Enhancers Using Stratum Corneum Lipid Liposomes: Preliminary Evaluation for Different Concentrations of Ethanol. J. Pharm. 2017, 1–10. https://doi.org/10.1155/2017/7409420

Schachter, M., 2005. Chemical, pharmacokinetic and pharmacodynamic properties of statins: an update. Fundam. Clin. Pharmacol. 19, 117–125. https://doi.org/10.1111/j.1472-8206.2004.00299.x

Shafaat, K., Kumar, B., Das, S.K., Ul Hasan, R., Prajapati, S.K., 2013. Novel nanoemulsion as vehicles for transdermal delivery of Clozapine: In vitro and in vivo studies. Int. J. Pharm. Pharm. Sci. 5, 126–134. https://doi.org/10.1016/j.nedt.2012.05.008

Shah, S.N.H., Tahir, M.A., Safdar, A., Riaz, R., Shahzad, Y., Rabbani, M., Karim, S., Murtaza, G., 2013. Effect of permeation enhancers on the release behavior and permeation kinetics of novel tramadol lotions. Trop. J. Pharm. Res. 12, 27–32. https://doi.org/10.4314/tjpr.v12i1.5

Shaker, D.S., Ishak, R.A.H., Ghoneim, A., Elhuoni, M.A., 2019. Nanoemulsion: A Review on Mechanisms for the Transdermal Delivery of Hydrophobic and Hydrophilic Drugs. Sci. Pharm. 87, 1-34 https://doi.org/10.3390/SCIPHARM87030017

Shaker, D., Nasr, M., Mostafa, M., 2013. bioavailability and hypocholesterolemic effect of proniosomal simvastatin for transdermal delivery. Int. J. Pharm. Pharm. Sci. 4, 344-351

Shaker, D.S., Sloat, B.R., Uyen M, L., Löhr, C. V., Yanasarn, N., Fischer, K.A., Cui, Z., 2007. Immunization by application of DNA vaccine onto a skin area wherein the hair follicles have been induced into anagen-onset stage. Mol. Ther. 15, 2037–2043.

Soujanya, C., Ravi Prakash, P., 2019. Formulation and Evaluation of Proniosomal Gel-Based Transdermal Delivery of Atorvastatin Calcium by Box–Behnken Design. Asian J. Pharm. Clin. Res.12, 335–343.

Subramanian, S., Keerthana Devi, M., Vaiyana Rajesh, C., Sakthi, M., Suganya, G., Ravichandran, S., 2016. Preparation, Evaluation, and Optimization of Atorvastatin Nanosuspension Incorporated Transdermal Patch. Asian J. Pharm. 10, 4, S487.

Suyal, J., Ganesh, B., 2017. An introductory review article on nanoemulsion. J. Pharm. Pharm. Sci. 2, 35–40.

Tadros, T.F., 2013. Emulsion formation, stability and reology. In: Emulsion formation and stability, pp. 1-75, Wiley-VCH Verlag GmbH & Co. KGaA. DOI:10.1002/9783527647941

Tenjarla, S., 1999. Microemulsions: an overview and pharmaceutical applications. Crit. Rev. Ther. Drug Carrier Syst. 16, 461–521.

Thakur, N., Garg, G., Sharma, P.K., Kumar, N., 2012. Nanoemulsions: A Review on Various Pharmaceutical Application. Glob. J. Pharmacol. 6, 222–225.

Van der Merwe, D., Riviere, J.E., 2005. Comparative studies on the effects of water, ethanol and water/ethanol mixtures on chemical partitioning into porcine stratum corneum and silastic membrane. Toxicol. Vitr. 19, 69–77. https://doi.org/10.1016/j.tiv.2004.06.002

Verma, A., Jain, A., Hurkat, P., Jain, S.K., 2016. Transfollicular drug delivery: current perspectives. Res. Reports Transdermal Drug Deliv. 5, 1–17. https://doi.org/10.2147/RRTD.S75809

Williams, A.C., Barry, B.W., 2012. Penetration enhancers. Adv. Drug Deliv. Rev. 64, 128–137.

Williams, D., Feely, J., 2002. Pharmacokinetic-pharmacodynamic drug interactions with HMG-CoA reductase inhibitors. Clin. Pharmacokinet. 41, 343–370. https://doi.org/10.2165/00003088-200241050-00003

Zhao, X., Liu, J.P., Zhang, X., Li, Y. 2006. Enhancement of transdermal delivery of theophylline using microemulsion vehicle. Int. J. Pharm. 327, 58-64.

Figure Captions:

Fig. 1. Pseudo-ternary phase diagram of different NE systems: (A) System I: OA/Tween 80/ PEG 400 (Smix 1:1), (B) System II: OA/Tween 80/ PEG 400 (Smix 2:1), (C) System III: OA/Tween 20/ PEG 400 (Smix 1:1), (D) System IV: OA/Tween 20/ PEG 400 (Smix 2:1), and (D) System V: OA/Tween 20/ PEG 400 (Smix 3:1). The shaded area indicates the region of stable NE formulae.

Fig. 2. *In vitro* release profiles of ATOR from formulae F1, F3, F6, F8 and F10.

Fig. 3. Representative TEM images of F1 (A), F8 (B), F1E (C) and F1EP (D)

Fig. 4. Skin permeation profiles of ATOR from different NE formulae.

Fig. 5. Permeation parameters of the optimized ATOR-loaded NE formulae.

Fig. 6. Mean ATOR plasma concentration–time curves (n = 6) after application of ATOR-loaded NE (F1EP) and ATOR in OA onto the dorsal rats' skin and after oral administration of ATOR dispersion at a single dose (80 mg/kg).

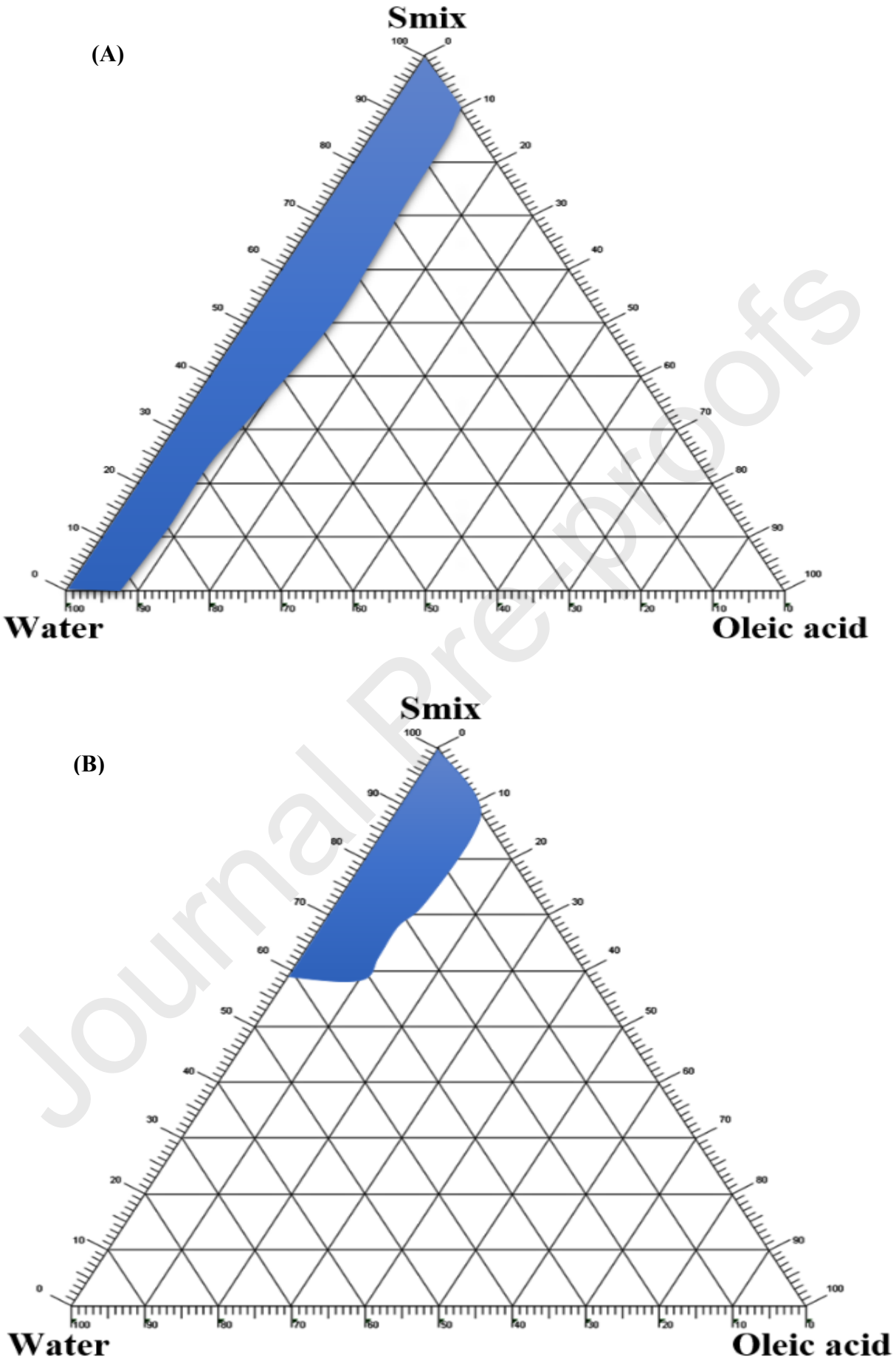

Fig. 1.

(C)

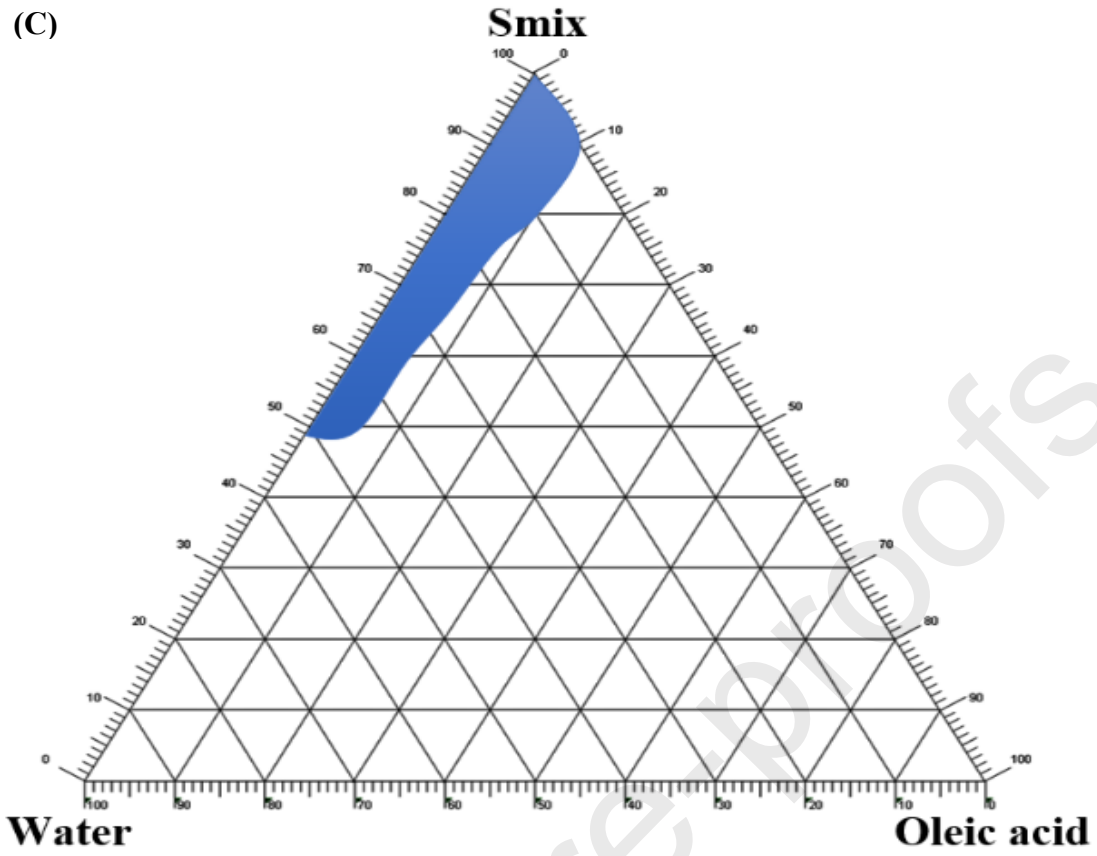

(D)

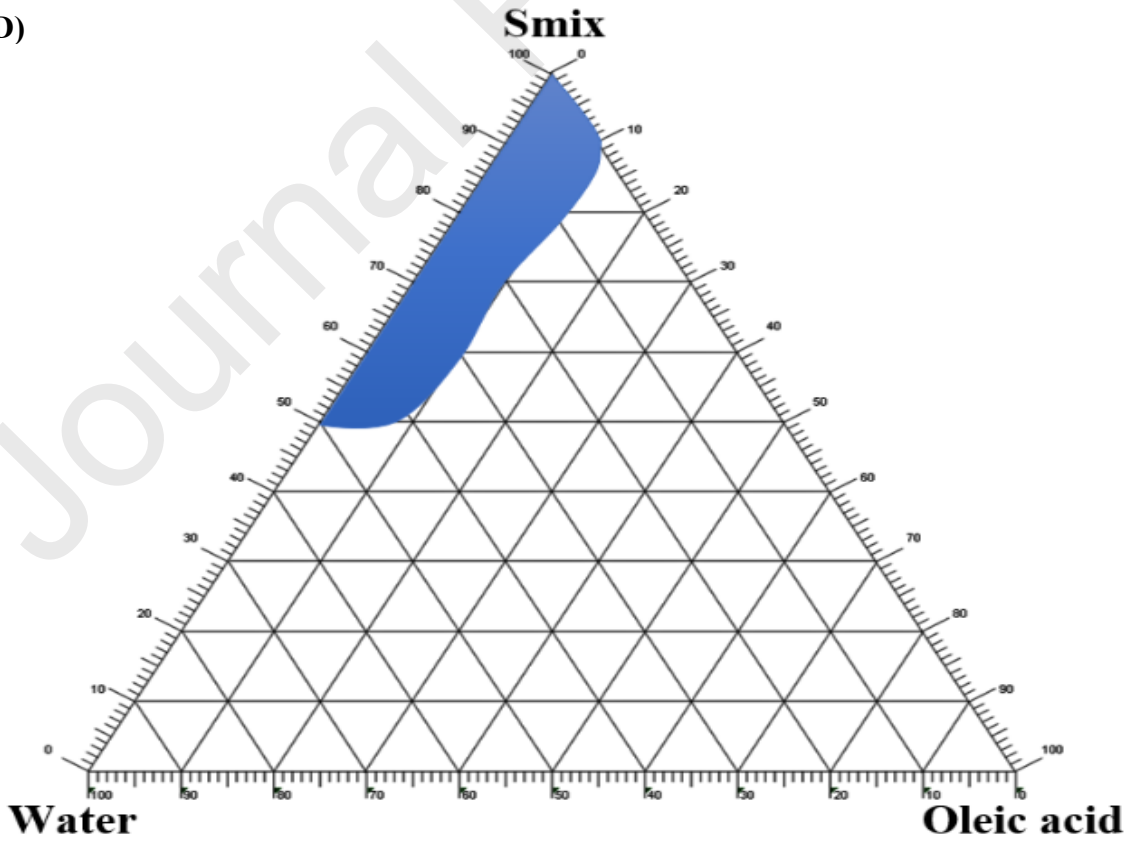

Fig. 1. (Cont.)

(E)

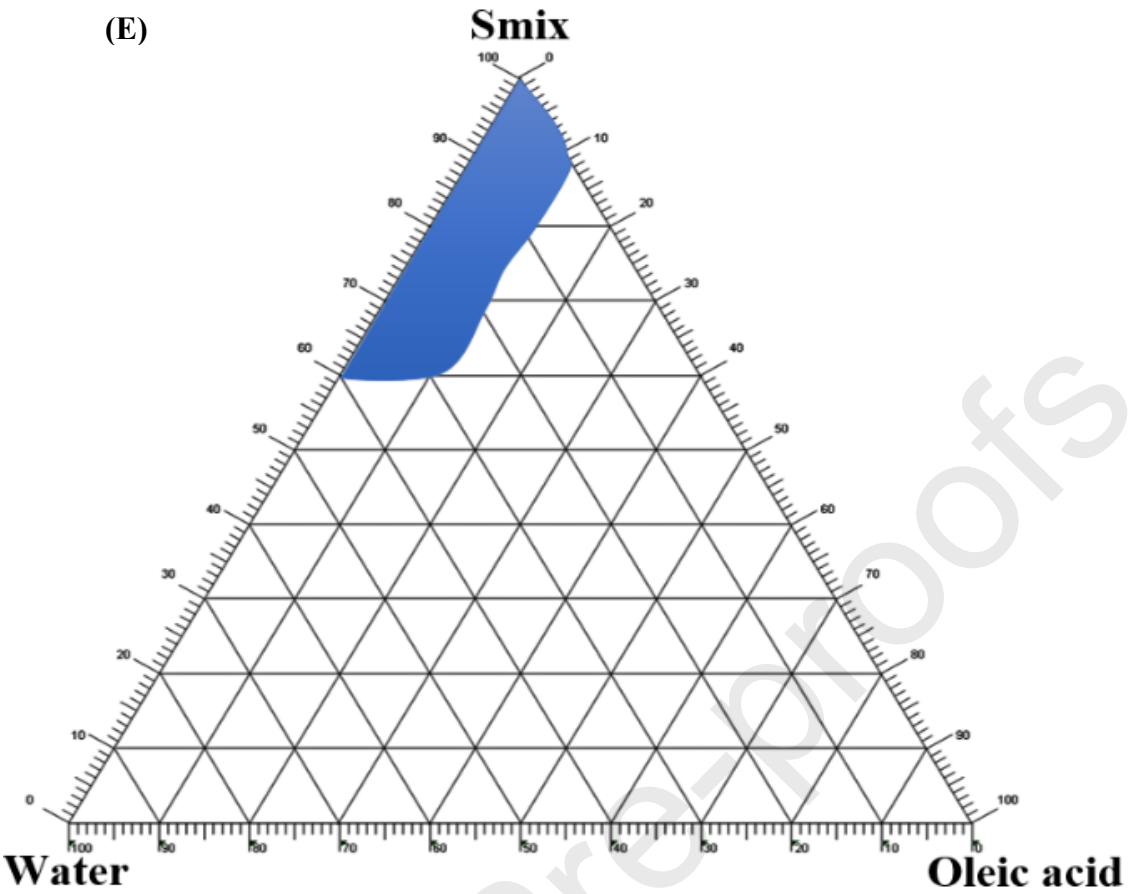

Fig. 1. (Cont.)

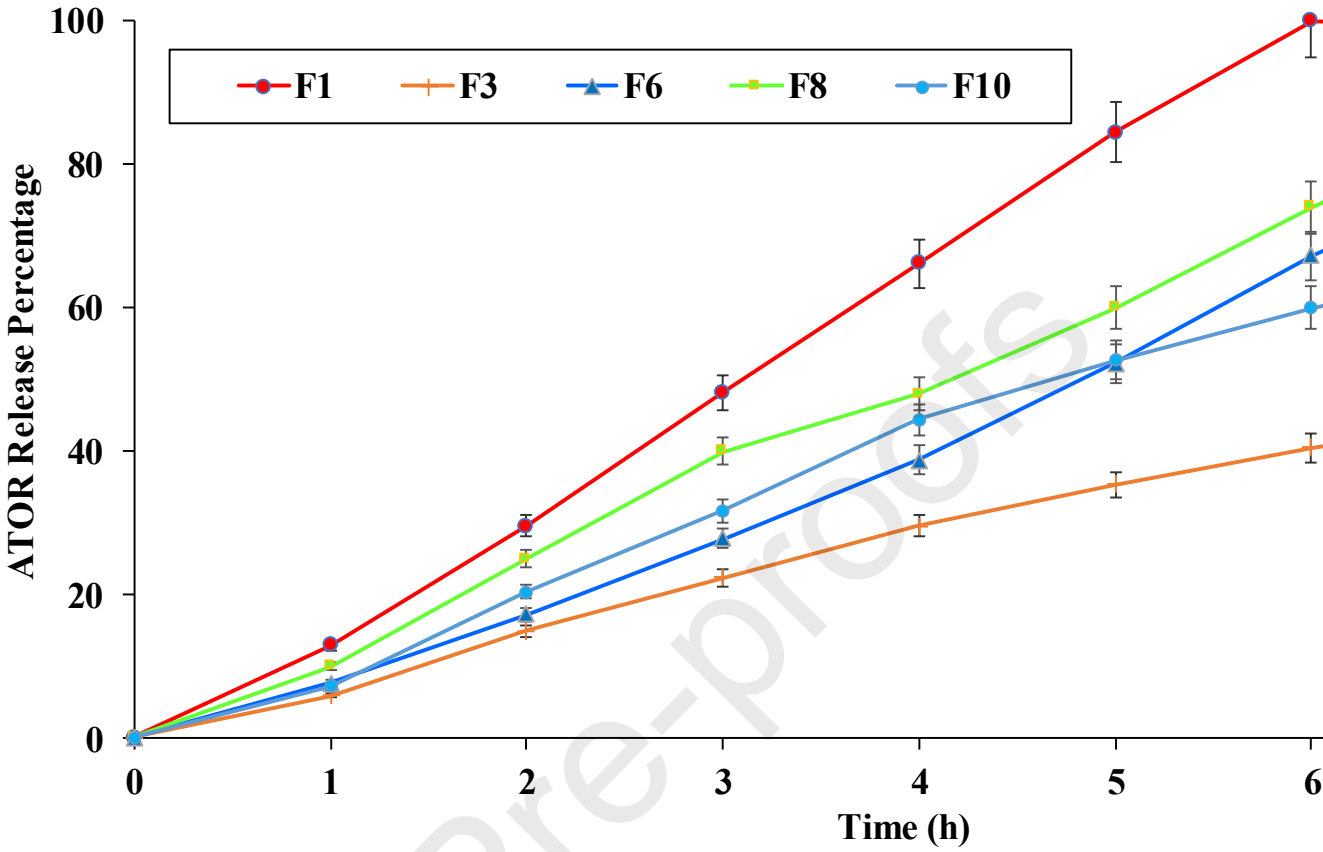

Fig. 2

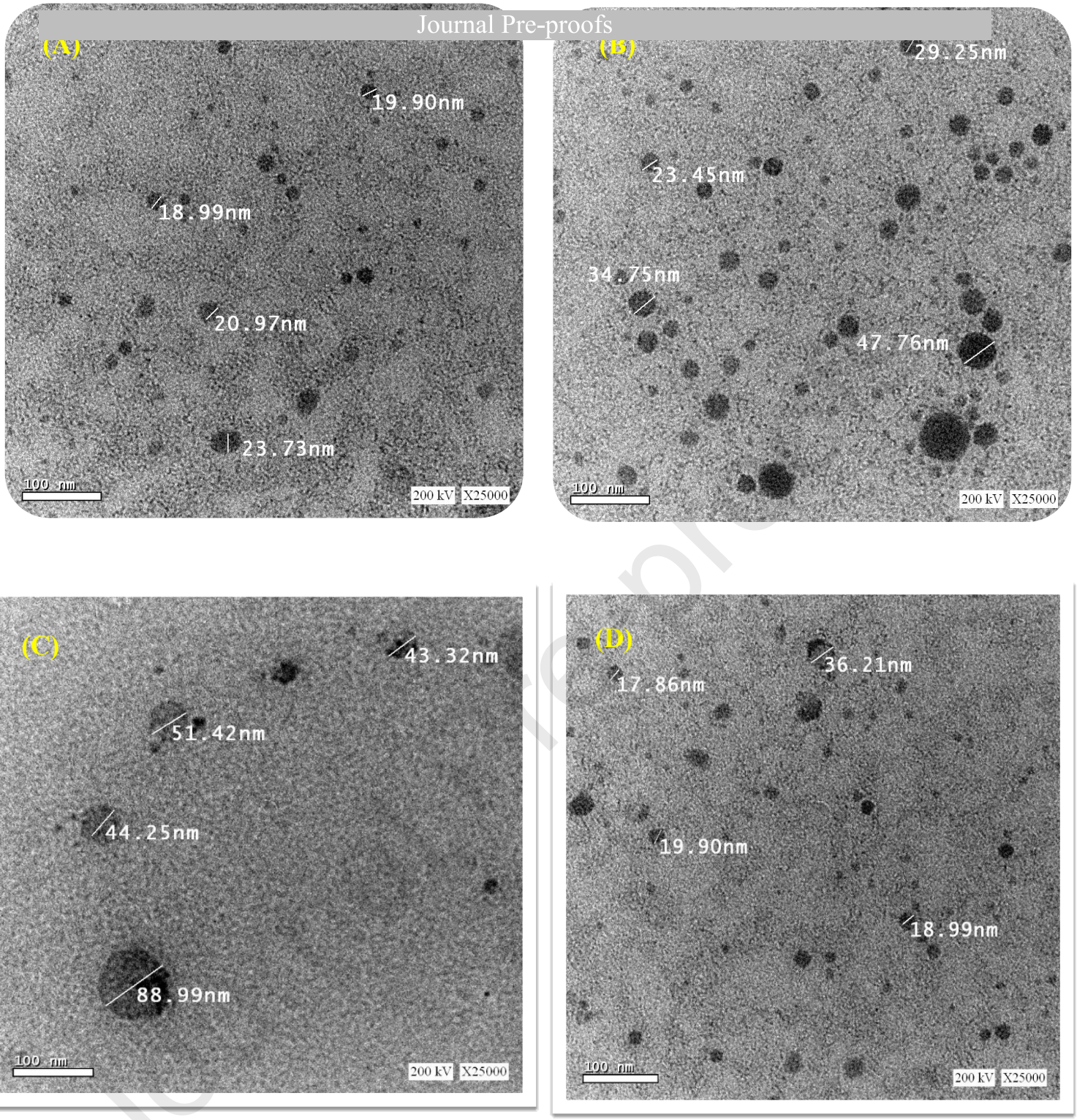

Fig. 3

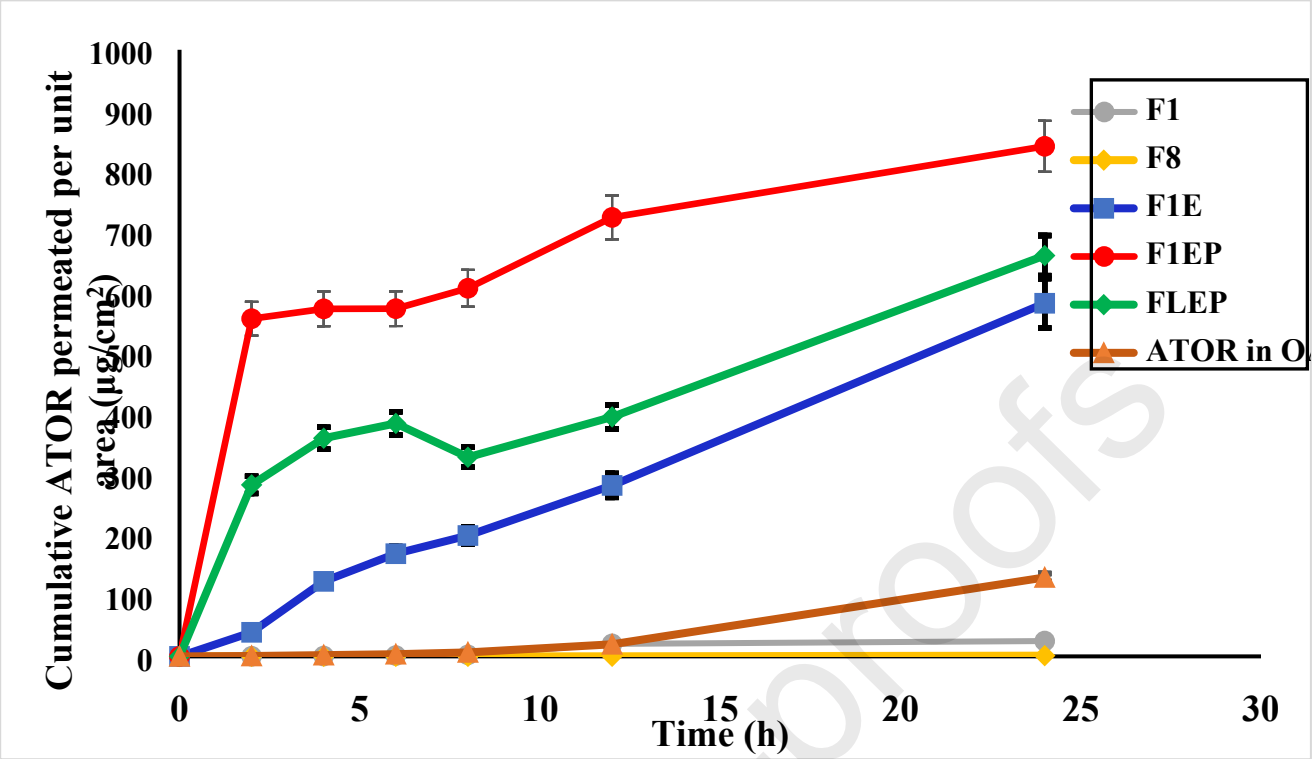

Fig. 4

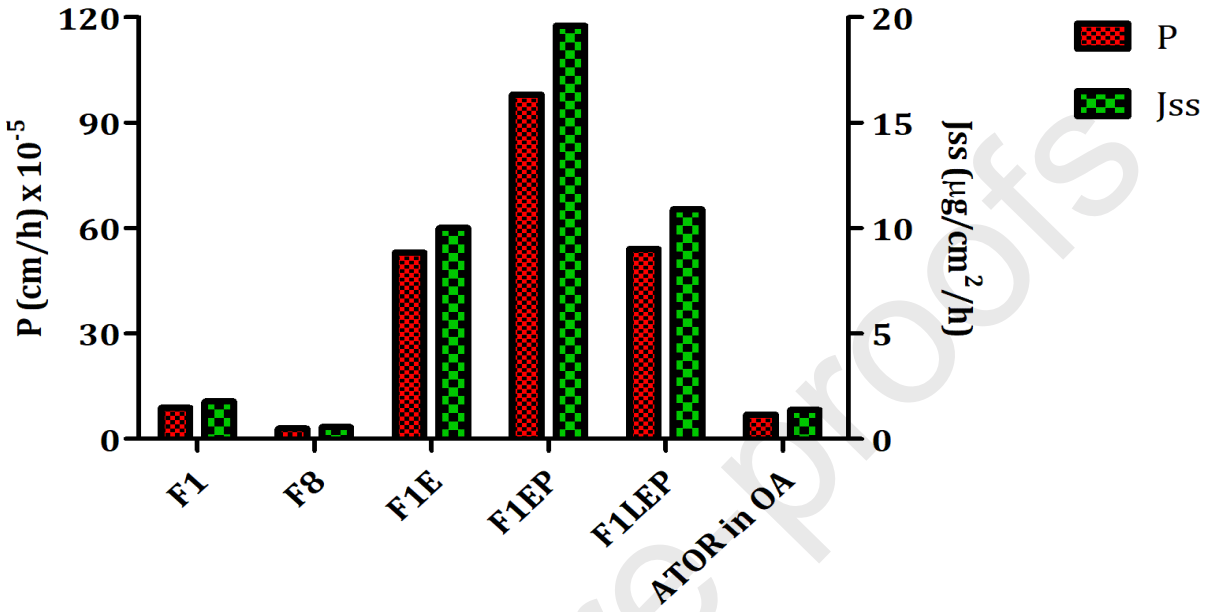

Fig. 5

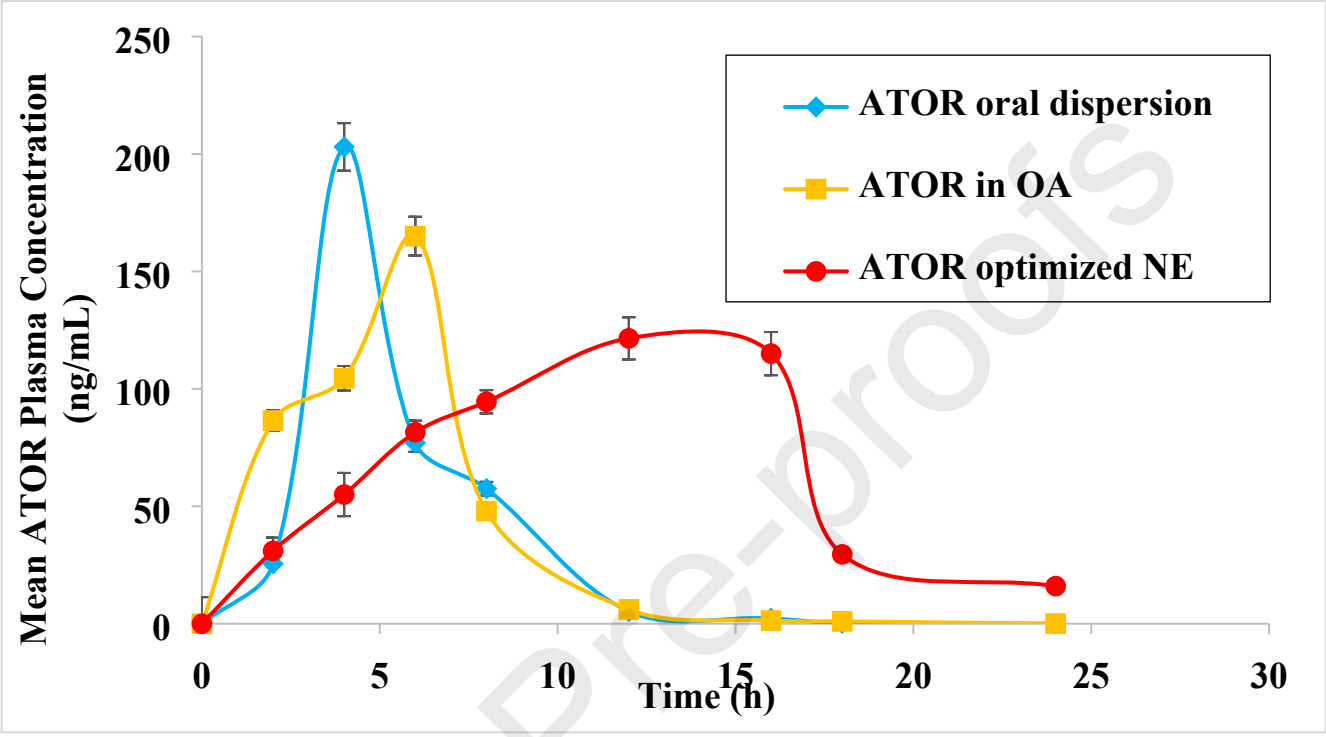

Fig. 6

Formula Code	Smix ratio	Composition (%w/w)					Droplet Size (nm) ± SD	PDI ± SD	ZP (mV) ± SD
		OA	Tween 80	Tween 20	PEG 400	Water			
F1	1:1	9	40.5	-	40.5	10	168.2 ± 12.3	0.28 ± 0.03	-20.0 ± 1.5
F2	2:1	7	42	-	21	30	194.3 ± 14.6	0.42 ± 0.07	-19.9 ± 0.65
F3	2:1	9	54	-	27	10	241.3 ± 20.3	0.34 ± 0.06	-19.6 ± 2.6
F4	1:1	6	-	27	27	40	185.2 ± 12.6	0.41 ± 0.03	-18.3 ± 0.94
F5	1:1	7	-	31.5	31.5	30	195.6 ± 14.3	0.62 ± 0.04	-30.0 ± 1.9
F6	1:1	9	-	40.5	40.5	10	142.4 ± 9.9	0.30 ± 0.01	-24.0 ± 2.6
F7	2:1	5	-	30	15	50	156.0 ± 12.2	0.25 ± 0.06	-15.0 ± 2.3

F8	2:1	9	-	53.5	27.5	10	142.5 ± 14.9	0.32 ± 0.09	-26.3 ± 0.2
F9	2:1	7	-	42	21	30	472.0 ± 19.6	0.19 ± 0.03	-18.0 ± 0.3
F10	3:1	9	-	60.7	20.3	10	111.8 ± 16.6	0.17 ± 0.02	-22.5 ± 0.4

Table 1. Composition and characteristics of the selected NE formulae.

N.B.: All data are average of 3 determinations.

Smix ratio: surfactant to co-surfactant ratio, OA: oleic acid, PDI: polydispersity index, ZP: zeta potential, SD: standard deviation.

Table 2. Composition and characteristics of the optimized NE formulae.

Formula Code	Composition (%w/ w)							Droplet Size (nm) ± SD	PDI ± SD	ZP (mV) ± SD	Viscosity (cPs) ± SD
	OA	Tween 80	Tween 20	PEG 400	Ethanol	Limonene	Water				
F1	9	40.5	-	40.5	-	-	10	168.2 ± 12.3	0.28 ± 0.03	-20.0 ± 1.5	309.1 ± 9.2
F8	9	-	53.5	27.5	-	-	10	142.5 ± 14.9	0.32 ± 0.09	-26.3 ± 0.2	282.6 ± 8.4
F1E	9	40.5	-	-	40.5	-	10	320.2 ± 14.3	0.19 ± 0.03	-13.0 ± 1.6	26.4 ± 0.3
F1EP	9	40.5	-	20	20.5	-	10	261.3 ± 14.6	0.41 ± 0.07	-15.4 ± 0.7	34.8 ± 0.6
F1LEP	9	40.5	-	10	25.5	5	10	241.3 ± 20.3	0.33 ± 0.06	-18.0 ± 2.2	38.2 ± 1.6

N.B.: All data are average of 3 determinations.
OA: oleic acid, PDI: polydispersity index, ZP: zeta potential, SD: standard deviation.

Table 3. Mean plasma TC levels before and after 7 days of treatment in hypercholesterolemic rats.

Group Code	Treatment	Mean plasma TC level (mg/dL ± SD, n = 6)		% Reduction in plasma TC level
		Before treatment	After treatment	
G-1	**F1**	145.8 ± 4.3	121.8 ± 6.3	16.5 ± 3.4
G-2	**F1E**	144.0 ± 8.1	115.4 ± 3.1	19.9 ± 2.8
G-3	**F1EP**	152.4 ± 5.6	111.2 ± 8.1	27.2 ± 2.6
G-4	**F1LEP**	166.4 ± 3.5	136.4 ± 6.3	18.0 ± 3.7
G-5	**ATOR in OA**	190.8 ± 9.3	169.0 ± 8.3	11.4 ± 2.9
G-6	**ATOR oral dispersion**	144.4 ± 6.2	122.8 ± 5.2	15.0 ± 3.7

Table 4. *In vivo* PK parameters after administration of ATOR NE (F1EP), ATOR in OA and ATOR oral dispersion to rats at a single dose of 80 mg/kg

PK Parameters	Mean data* ± SD		
	ATOR NE (F1EP)	ATOR in OA	ATOR Oral Dispersion
T_{max} (h)	12 (12-16)*	5.5 (4-6)*	4 (2-6)*
C_{max} (ng/mL)	121.5 ± 4.9	165 ± 35.3	203.0 ± 18.3
AUC $_{0-24}$ (ng.h/mL)	1695 ± 172.2	884.3 ± 151.2	790.8 ± 151.3
MRT (h)	11.3 ± 0.1	5.4 ± 0.3	6.7 ± 0.2
Relative Bioavailability (%)	214.3	111.8	---

*median T_{max} (max-min)

Dalia S. Shaker: **Conceptualization, Data curation, Methodology, Software**

Rania A. H. Ishak.: Data curation, Writing- Original draft preparation.

Muaeid A Elhuoni: Visualization, Investigation.

Amira M. Ghoneim: Data curation, Software, Validation, Writing- Reviewing and Editing

Declaration of interests

☒ The authors declare that they have no known competing financial interests or personal relationships that could have appeared to influence the work reported in this paper.

☐The authors declare the following financial interests/personal relationships which may be considered as potential competing interests: